Supplementary Material

Microstructure-property relationships in composites of 8YSZ ceramics and *in situ* graphitized nanocellulose

Polona Hudelja[1,2] Rainer Schmidt[3,4], Harvey Amorín[5], Sandra Drev[6], Aljaž Iveković[1], Anže Abram[1], Andraž Kocjan*[,1], Bernd Wicklein[5]

[1] *Department for Nanostructured Materials, Jožef Stefan Institute, Jamova 39, 1000 Ljubljana, Slovenia.*

[2] *Jožef Stefan International Postgraduate School, Jamova 39, 1000, Ljubljana, Slovenia*

[3] *Facultad de Ciencias Físicas, GFMC, Universidad Complutense de Madrid, 28040 Madrid, Spain.*

[4] *Laboratorio de Heteroestructuras con aplicación en spintrónica, Unidad asociada UCM/CSIC, 28049 Madrid, Spain.*

[5] *Materials Science Institute of Madrid (ICMM), Consejo Superior de Investigaciones Científicas (CSIC), Sor Juana Inés de la Cruz 3, 28049 Madrid, Spain.*

[6] *Center for Electron Microscopy and Microanalysis, Jožef Stefan Institute, Jamova 39, SI-1000 Ljubljana, Slovenia*

Corresponding author: Andraz Kocjan, e-mail: a.kocjan@ijs.si

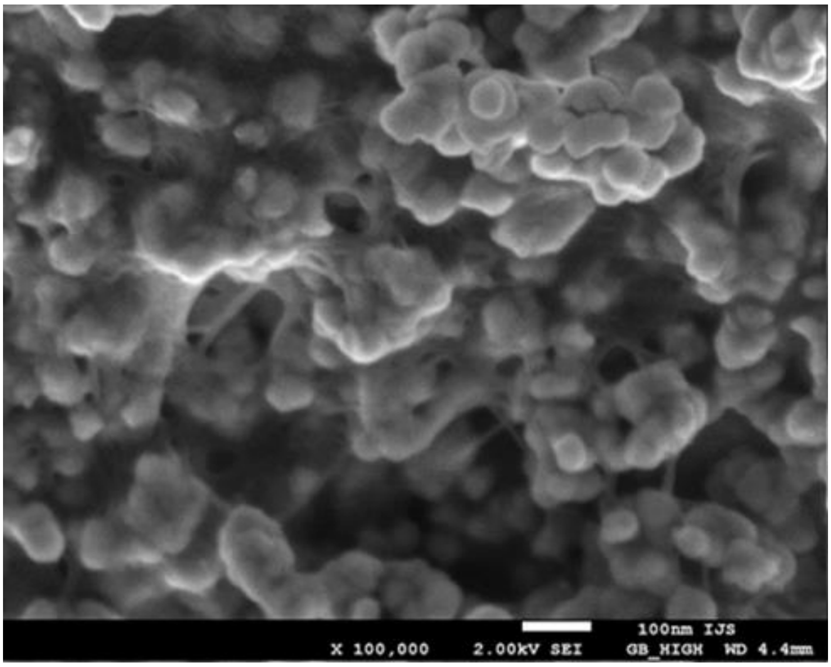

Figure S1. Scanning Electron Microscopy (SEM) micrograph showing a typical microstructure of the freeze-dried 8YSZ powder containing cellulose nanofibers (CNF). 8YSZ nanocrystallites (~80 nm) are embedded in a CNF network (sample 8Y-2CNF).

Table S1. d_{10}, d_{50} and d_{90} values extracted from cumulative grain size distributions (Figure 4, main text) for the SPS sintered 8Y and 8Y-xCNF samples.

Sample name	d_{10}	d_{50}	d_{90}
8Y-1200	0.08	0.18	0.31
8Y-0.75CNF-1200	0.07	0.13	0.23
8Y-1CNF-1200	0.08	0.14	0.25
8Y-2CNF-1200	0.07	0.13	0.22
8Y-1400	0.60	1.60	2.69
8Y-0.75CNF-1400	0.18	0.40	0.67
8Y-1CNF-1400	0.20	0.58	1.10
8Y-2CNF-1400	0.15	0.30	0.52
8Y-1600	1.39	4.92	8.22
8Y-0.75CNF-1600	1.29	3.33	5.41
8Y-1CNF-1600	0.35	0.86	1.51
8Y-2CNF-1600	0.17	0.52	1.03

Table S2. FWHM values (in cm^{-1}) of the D, G and 2D bands of sintered 8Y-*x*CNF.

	D	**G**	**2D**
8Y-0.75CNF	46	43	77
8Y-1CNF	46	47	81
8Y-2CNF	50	49	88

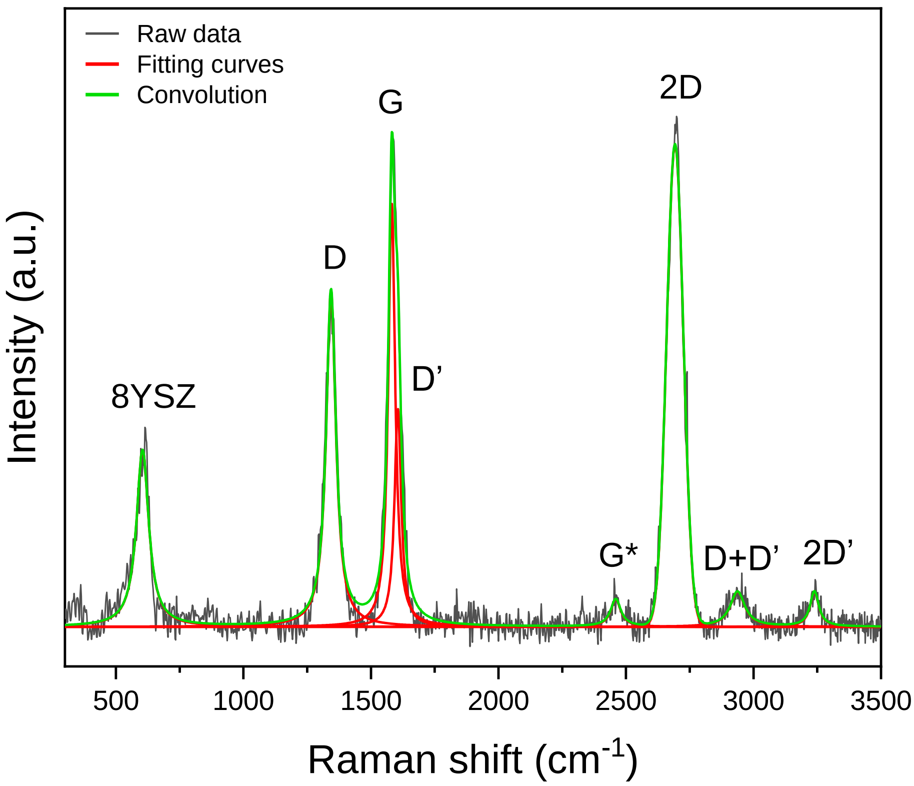

Figure S2. Lorentz fitting curves of Raman spectrum from 8Y-0.75CNF sintered at 1400 °C.

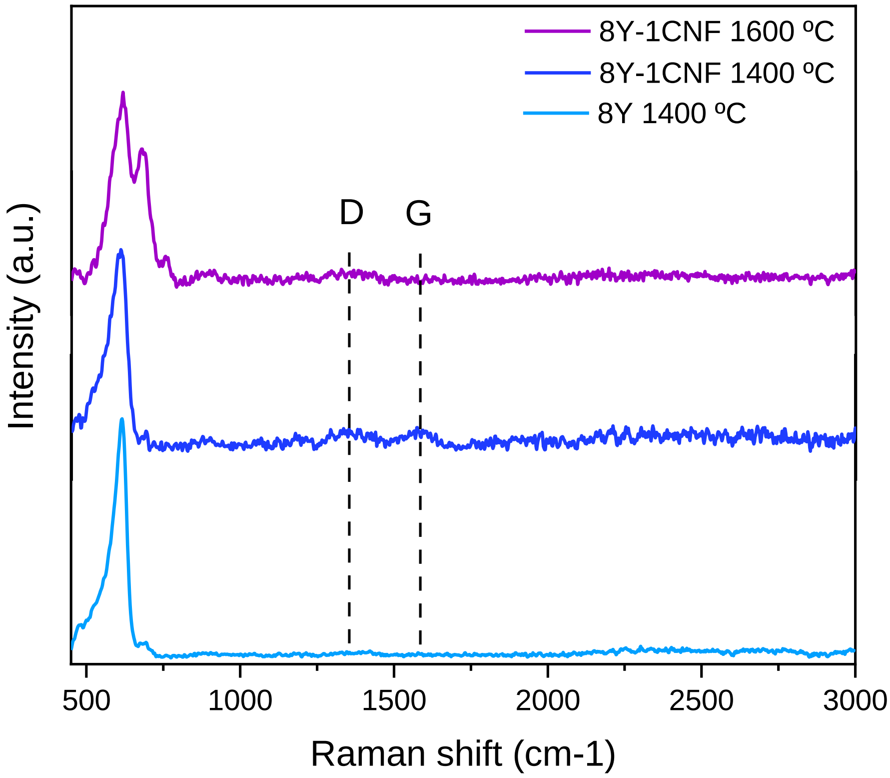

Figure S3. Raman spectra of 8Y and 8Y-1CNF sintered in a conventional furnace.

Supplementary discussion of dielectric data.

The dielectric data in the format of the dielectric permittivity ε' vs frequency (*f*) for all measurement temperatures are shown in Fig. S4a-c for the 0 %, 0.75 % and 1 % CNF samples. The bulk and GB contributions can be identified readily in form of two approximately *f*-independent plateaus (Bulk, GB), whereas the interface blocking at low *f* is manifested by a linear increase of *ε'* with decreasing *f* (IF). Interestingly, the 1% CNF sample shows a slight downturn of the *ε'* vs *f* curves at the high *f* end, where the trend seems to be absent for the 0 and 0.75 % samples. This downturn can be associated with the graphite phase and could in fact be accounted for in the equivalent circuit model by an additional R-CPE element in series as mentioned in the main text (see also Fig. 8c in the main text).

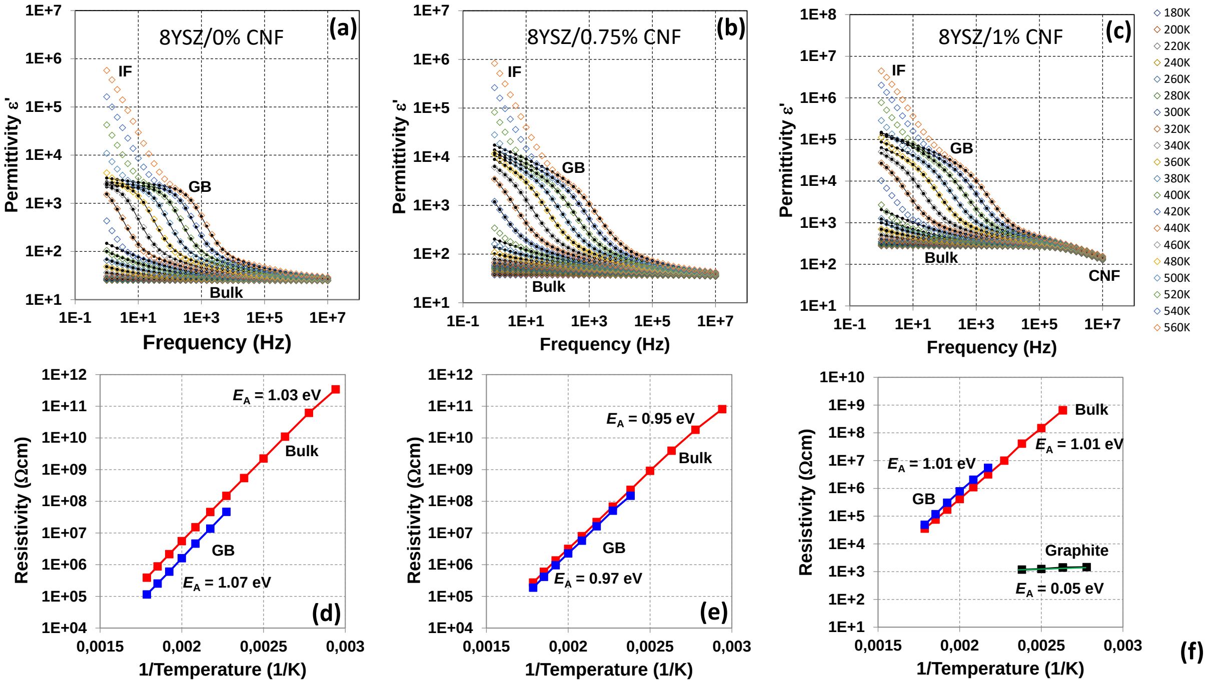

Figure S4. Dielectric data from 8Y-*x*CNF with x = 0, 0.75, 1 sintered at 1400 °C plotted in the format of *ε'* vs. *f* plots at various temperatures as indicated in the legend at the right side of the graphs (a-c). Open symbols correspond to the data, solid squares and lines to the fits using the equivalent circuits shown in the Fig. 9a-c (insets) of the main text. Resistivity values obtained from the bulk and GB resistors in the equivalent circuit models plotted on logarithmic axes vs. 1/*T* (d-f). The respective charge transport activation energies are indicated. Note that Figure S4f is equivalent to Figure 11 in the main text.

Furthermore, the trends of resistivity vs 1/T are shown in Fig.S4d-f for the 0, 0.75 and 1.0 % samples. The trends of decreasing resistivity with increasing initial CNF content were associated with the conducting character of the ex-CNF graphite phase, which may act as an internal electrode that can short-circuit several grains, as mentioned in the main text. Furthermore, the relative increase of the GB resistivity in comparison to the bulk contribution with increasing CNF was interpreted as a result of the decreasing grain size and the graphite accumulating at the GBs to cause higher resistivity, which had also been discussed in the main text. The data is plotted on semi-logarithmic axes of resistivity (Ωcm) vs 1/T (1/K). Good linearity is indicated, which points towards thermally activated charge transport. The activation energies E_A were determined from the corresponding Arrhenius plots (figures not shown). The activation energy may be slightly lower in the 0.75% CNF sample, which may be attributed to an improved densification sintering effect. However, the effect is small as compared to the experimental limitations and should probably not be overinterpreted.